CFD SIMULATION OF PRESSURE REDUCTION INSIDE LARGE-SCALE LIQUEFIED HYDROGEN TANK

Tani, K.[1], Himeno, T.[2], Watanabe, T.[3], Kobayashi, H.[4], Toge, T.[5], Unno, S.[6], Kamiya, S.[7], Muragishi, O.[8], and Kanbe, K.[9]

[1] School of Engineering, The University of Tokyo, 7-3-1 Hongo, Bunkyo-ku, Tokyo, 113-8654, Japan, tani@aero.t.u-tokyo.ac.jp

[2] Department of Aeronautics and Astronautics, The University of Tokyo, 7-3-1 Hongo, Bunkyo-ku, Tokyo, 113-8654, Japan, himeno@aero.t.u-tokyo.ac.jp

[3] Department of Aeronautics and Astronautics, The University of Tokyo, 7-3-1 Hongo, Bunkyo-ku, Tokyo, 113-8654, Japan, watanabe@aero.t.u-tokyo.ac.jp

[4] Institute of Space and Astronautical Science, Japan Aerospace Exploration Agency, 3-1-1 Yoshinodai, Chuo-ku, Sagamihara City, Kanagawa Prefecture, 252-5210, Japan, kobayashi.hiroaki@jaxa.jp

[5] Kawasaki Heavy Industries, Ltd., 1-1, Kawasaki-cho, Akashi City, 673-8666, Japan, toge_terukuni@khi.co.jp

[6] Kawasaki Heavy Industries, Ltd., 1-1, Kawasaki-cho, Akashi City, 673-8666, Japan, kagaya@khi.co.jp

[7] Kawasaki Heavy Industries, Ltd., 1-1, Kawasaki-cho, Akashi City, 673-8666, Japan, kamiya_s@khi.co.jp

[8] Kawasaki Heavy Industries, Ltd., 1-1, Kawasaki-cho, Akashi City, 673-8666, Japan, muragishi_osamu@khi.co.jp

[9] Kawasaki Heavy Industries, Ltd., 1-1, Kawasaki-cho, Akashi City, 673-8666, Japan, kanbe_k@khi.co.jp

ABSTRACT

Building the international hydrogen supply chain requires the large-scale liquefied hydrogen(LH2) carrier. During shipping LH2 with LH2 Carrier, the tank is pressurized by LH2 evaporation due to heat ingress from outside. Before unloading LH2 at the receiving terminal, reducing the tank pressure is essential for the safe tank operation. However, pressure reduction might cause flashing, leading to rapid vaporization of liquefied hydrogen, liquid leakage. Moreover, it was considered that pressure recovery phenomenon which was not preferred in terms of tank pressure management occurred at the beginning of pressure reduction. Hence, the purpose of our research is to clarify the phenomenon inside the cargo tank during pressure reduction. The CFD analysis of the pressure reduction phenomenon was conducted with the VOF based in-house CFD code, utilizing the C-CUP scheme combined with the hybrid Level Set and MARS method. In our previous research, the pressure reduction experiments with the 30 m^3 LH2 tank were simulated, and the results showed that the pressure recovery was caused by the boiling delay, and the tank pressure followed the saturation pressure after the liquid was fully stirred. In this paper, the results were re-evaluated in terms of temperature. While pressure reduction was dominant, the temperature of vapor-liquid interface decreased. Once the boiling bubble stirred the interface, its temperature reached the saturation temperature after pressure recovery occurred. Moreover, it was found that the liquid temperature during pressure reduction could not be measured because of the boiling from the wall of the thermometer. The CFD analysis on pressure reduction of 1250 m^3 tank for the LH2 Carrier was also carried out, and showed that the pressure recovery could occur in the case of the 1250 m^3 tank in a certain condition. These results provide new insight into the development of the LH2 carrier.

1. INTRODUCTION

The large-scale storage and transportation of hydrogen will play an important role in a future hydrogen society. One of the hydrogen storage and transportation technology is liquefied hydrogen[1]. Liquefied

hydrogen has a density of about 800 times that of gaseous hydrogen at room temperature and atmospheric pressure. The high gravimetric and volumetric efficiencies of liquefied hydrogen make it suitable for large-scale hydrogen storage and transportation.

In 2017, Japanese government had determined the Basic Hydrogen Strategy for building the hydrogen society. This strategy aimed to establish the commercial supply chains by 2030 and increase the hydrogen distribution from 200 tons in 2017 to 300,000 tons in 2030[2]. One of the commercial supply chains was the Hydrogen Energy Supply Chain (HESC) (Fig.1) [3]. This project planned to employ the liquefied hydrogen to store and transport a large amount of hydrogen. In the HESC, a large amount of liquefied hydrogen was produced from brown coal in Australia and transported to Japan on the liquefied hydrogen carrier. For these backgrounds, Kawasaki Heavy Industries, Ltd. has developed and built the first large-scale liquefied hydrogen carrier(Table 1) called SUISO FRONTIER[4],[5],[6]. In this demonstration test, the carrier with a 1,250m^3 tank would be loaded with liquefied hydrogen. The technical verification of the long-distance and large-scale transportation and cargo handling of liquefied hydrogen would be conducted.

SUISO FRONTIER owned the double-shell structure of a cylindrical horizontal storage tank. Austenitic stainless steel which did not decrease the strength and toughness under cryogenic conditions was used for the tank material, and the space between the inner and outer shells had a multi-layer vacuum insulation structure for reducing the amount of boil-off gas. In addition, inner shell of the tank was supported by GFRP (Glass Fiber Reinforced Plastic) structure, and Kawasaki Panel insulation System(KPS) was built into the outer shell as an auxiliary insulation mechanism[5]. In the demonstration test, the measurement of this insulation efficiency and the safe transportation method will be verified.

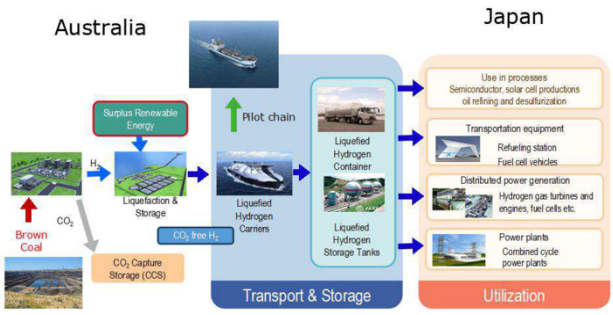

Fig. 1 CO_2-free Hydrogen Energy Supply Chain (HESC) project. LH2 will be produced from brown coal in Australia and transported to Japan by using LH2 carriers (LH2Cs) [3].

Table 1 Specification of the LH2 Carrier "SUISO FRONTIRE" [4]

Ship	
Principal Dimensions	L x B x D (ab. 110m x ab.20m x ab.11m)
Gross Tonnage	Ab. 8,000
Propulsion System	Diesel-electric
Speed	Ab.13.0 knots
Flag State/Class	Japan / Nippon Kaiji Kyokai(Class NK)
Cargo Containment System	
Total Capacity	Ab. 1250m3(No. of Tank: 1)
Tank Type	IMO Independent Tank Type C
Max. Design Pressure	0.4MPaG
Min. Design Temperature	-253 degree C (20K)
Insulation System	Multi-layer Vacuum Insulation Structure + Supplementary Kawasaki Panel Insulation System
BOG Management	Pressure Accumulation in the inner vessel in principle

Due to heat input during long transportation, the entire liquid phase got saturated with a high liquid level and high pressure in Japan, thus it was required to reduce the tank pressure for safe unloading operation. However, when the saturated liquid experiences pressure reduction, it leads to boil and generate the large amounts of gas because of saturation temperature drop. As Fig.2 showed, the pressure reduction operation before unloading had an event of excess capacity of the vent system and liquid spillage caused by massive vapor generation. Our research focused on this depressurization issue with regard to the unloading operation.

The boiling at reduced pressure was called flashing or flash evaporation, and this phenomenon has been used in the industrial application, such as seawater desalination and loss-of-coolant accidents (LOCA) of pressurized water nuclear reactors. In studies on pool flashing in a tank, Miyatake et al. [7], [8] conducted flashing experiments with water, summarizing the mechanism and visualization results. It was found that flash evaporation experienced two processes in which the phenomenon decays exponentially with time. Also, the definitions of flash evaporation time, non-equilibrium fraction (NEF) and non-equilibrium temperature difference (NETD) and the experimental equations were proposed. Saury et al.[9], [10] revealed that the liquid level affected the boiling depth, flash evaporation time and evaporation mass by considering the energy balance of water flash evaporation. From the experiments under various initial conditions, it was suggested that the initial temperature, overheating temperature, pressure reduction rate, initial liquid level and the liquid surface affected flashing. Zhang et al.[11] analyzed the main influencing factors of flash evaporation efficiency and the steam-carrying for water and NaCl solutions. The steam-carrying ratio was defined as the mass ratio of be-carried liquid and generated steam, and this ratio increased with the decreasing of separating height or the rising of initial liquid concentration. In addition, Wang et al.[12] attempted to describe the mechanism of flashing by using the thermodynamic model, comparing with the water flashing test. This thermodynamic model assumed that the phenomenon went through four physical processes, the exhaust from the tank, mild evaporation, flash evaporation of the liquid, and renewal of the void ratio in the tank. The results of the model analysis were in good agreement with the experimental results.

Flashing of cryogenic fluids had been studied by Hewitt and Parker[13] on bubble growth and collapse under rapid depressurization with liquid nitrogen, and they reported that the bubble behavior of liquid nitrogen was similar to that of non-cryogenic fluids. Yokoyama et al.[14] analyzed liquid nitrogen flashing considering thermal stratification, and visualized boiling behavior and measured pressure and temperatures. In this study, it was experimentally confirmed that a relatively hot gas-liquid interface boiled at the start of depressurization and then gradually generated vapor over the bottom of the vessel, and a large number of bubbles pushed up the entire liquid surface and recover the pressure of the vessel. Watanabe et al.[15], [16] developed thermodynamic model which was in good agreement with flashing experiment under thermal stratification condition. Moreover, they experimentally suggested that rapid pressure reduction caused vapor condensation which prevented non-equilibrium state. In addition, Takeda et al. [17] conducted flashing experiments with liquid nitrogen and clarified that pressure recovery phenomenon was affected by pressure reduction rate and liquid temperature.

However, the research on liquefied hydrogen flashing was still in progress, and the previous studies focused on utmost about 0.1 m^3 small tanks. The experimental correlations in the previous research might not be applicable for large-scale tank, because tank size was much larger than boiling bubble size and the tank pressure was less susceptible to volume changes caused by boiling nucleation. Moreover, it was considered that thermal properties and temperature distribution inside tank were possible to make a difference to the flashing phenomenon. Hence, the research on flashing

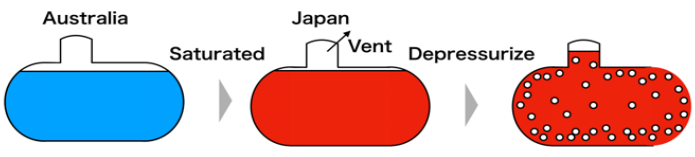

Fig. 2 Schematic of liquid state inside the Liquefied Hydrogen Carrier during shipping. [19]

phenomenon with large-scale liquid hydrogen tank were important for predicting the phenomenon inside the tanks for the Liquefied Carrier.

In our previous researches[18],[19], the world's first detailed measurements inside 30m3 large-scale liquefied hydrogen tank were performed, and the thermodynamic model for predicting the phenomenon inside the tank was developed. Also, it was revealed that pressure recovery phenomenon occurred at the high liquid level condition. This phenomenon might not be preferred in terms of the safe tank management. For investigating this unsteady phenomenon, the Computational Fluid Dynamics (CFD) analysis was conducted, and the 2-D and 3-D results showed that the pressure decrease was dominant at the beginning of the depressurization because of the lack of boiling from the wall. Then, the pressure increased with the increase of the vapor-liquid interfacial area due to boiling, and finally reached the equilibrium state. However, in these analyses, the pressure reduction phenomenon was not evaluated in terms of temperature. Moreover, the target was not the 1250 m^3 tank of SUISO FRONTIER but $30m^3$ liquefied hydrogen tank located at the JAXA Noshiro Rocket Testing Center, thus the safe depressurization operation had not been understood yet. For establishing safe depressurization operation, the purpose of this paper was to investigate the mechanism of the pressure recovery phenomenon in terms of temperature inside the large-scale liquefied hydrogen tank and clarify the phenomenon during the depressurization operation of SUISO FRONTIER.

2. NUMERICAL METHOD

2.1 Flow equations

To investigate the depressurization phenomenon, we conducted the CFD analysis. The free surface numerical method (CIP-LSM: CIP-based level set & MARS) developed by Himeno et al[20][21] and Umemura et al[22], [23] was employed in this research. Similarity to the CLSVOF(Coupled Level Set Volume-Of-Fluid) method[24], the CIP-LSM combined the VOF and the level-set method[25] for preventing the numerical diffusion of the vapor-liquid interface and tracking it with high accuracy, and calculated a phase change by assuming local equilibrium.

The governing equations for homogeneous two-phase flow consisted of mass, momentum, and internal energy equations, and could be described as followed.

$$\begin{aligned} &\frac{D\rho}{Dt} = -\rho\nabla\cdot\vec{u} \\ &\rho\frac{D\vec{u}}{Dt} = -\nabla p + \nabla(\mathbf{T_v} + \mathbf{T_\sigma}) + \rho\vec{g} \\ &\rho\frac{De}{Dt} = -p\nabla\cdot\vec{u} + \dot{\Theta} \end{aligned} \tag{1}$$

$$\mathbf{T_v} = -\frac{2\mu}{3}(\nabla\cdot\vec{u})\mathbf{I} + \mu\left(\mathbf{D} + \mathbf{D}^{\mathrm{T}}\right),$$

$$\mathbf{D} = \nabla\vec{\mathrm{u}},$$

$$\mathbf{T_\sigma} = \sigma\delta_s(\mathbf{I} - \overrightarrow{n_s}\overrightarrow{n_s}),$$

$$\dot{\Theta} = (\mathbf{T_v} + \mathbf{T_\sigma})\nabla\cdot\vec{u} - \nabla\cdot\vec{q}.$$

$$\frac{DH_s}{Dt} = \frac{\partial H_s}{\partial t} + (\vec{u}\cdot\nabla)H_S = 0, \tag{2}$$

$$\begin{aligned} &H_S = 0.5 \quad Liquid \\ &H_S = 0 \quad Interface \\ &H_S = -0.5 \quad Gas \end{aligned} \tag{3}$$

where t - time, s; ρ - density, kg/m^3; $\vec{u}$ - velocity, m/s; p - pressure, Pa; e - internal energy, J/kg; μ - dynamic viscosity coefficient, Pa·s; σ - surface tension, N/m; δ_s - Dirac's delta function, 1/m; $\vec{n}_s$ - normal vector at the interface, -; $\vec{q}$ - heat flux, W/m^2; H_s - Heaviside function, -.

These equations consisted of a fluid solution part for solving Eq. (1) and an interface tracking part for solving Eq. (2) which meant the advection equation for H_s function to distinguish between gas and liquid. If the void ratio was more than 50%, it was considered as a gas cell, while if it is less than 50%, the cell was treated as a liquid one in our simulation method.

The fluid solution part was solved by TCUP (Thermo CIP-CUP) method[21] with temperature as an independent variable. TCUP method was a kind of CIP-CUP method[26]. Based on TCUP method, Eq. (1) could be transformed into Eq. (4) with the basic quantity $Q = (u, T, p)^T$ as the state quantity. For conducting the phase change calculation, the phase change term was added, and the analysis was done using the following equations, which were rewritten in the equations for velocity, temperature, and pressure.

$$\begin{aligned}
&\rho\frac{D\vec{u}}{Dt} = -\nabla p + \nabla(\mathbf{T_\nu} + \mathbf{T_\sigma}) + \rho\vec{g} + \left(\vec{u}_{gas} - \vec{u}_{liq}\right)\dot{m}\delta_s \\
&\rho C_p\frac{DT}{Dt} = -T\frac{\rho_T}{\rho}\frac{Dp}{Dt} + \dot{\Theta} - \left\{h_{gas} - h_{liq} - p\left(\frac{1}{\rho_{gas}} - \frac{1}{\rho_{liq}}\right)\right\}\dot{m}\delta_s \\
&\frac{1}{\rho C_s^2}\frac{Dp}{Dt} = -\nabla\cdot\vec{u} - \frac{\rho_T}{\rho}\frac{\dot{\Theta}}{\rho C_p} - \left(\frac{1}{\rho_{gas}} - \frac{1}{\rho_{liq}}\right)\dot{m}\delta_s
\end{aligned} \tag{4}$$

where t - time, s; ρ - density, kg/m^3; $\vec{u}$ - velocity, m/s; p - pressure, Pa; $\dot{m}$ – phase change rate per unit area, kg/m^2/s; T - temperature, K; C_p - specific heat at constant pressure, J/kg/K; δ_s - Dirac's delta function, 1/m; h - enthalpy, J/kg; C_s – sound speed, m/s.

In these equations, the terms generated by considering the phase change indicated, in order, momentum loss and production, latent heat, and volume divergence due to gas-liquid density difference.

$$\begin{aligned}
&\left(\vec{u}_{gas} - \vec{u}_{liq}\right)\dot{m}\delta_s\,, \\
&-\left\{h_{gas} - h_{liq}\right\}\dot{m}\delta_s\,, \\
&-\left(\frac{1}{\rho_{gas}} - \frac{1}{\rho_{liq}}\right)\dot{m}\delta_s\,,
\end{aligned} \tag{5}$$

In the TCUP method, the fluid governing Eq. (4) were roughly divided into an advection term, which estimated the fluid derivative term on the left-hand side and a non-advection term on the right-hand side. In the advection term, the value of each state quantity was updated by the Constrained Interpolation Profile Scheme (CIP), which was a high-order accurate finite difference method for solving hyperbolic partial differential equations proposed by Yabe et al. [26]. The non-advection term was solved in two stages: a diffusion stage where the viscosity and heat transfer terms were evaluated implicitly and the velocity and temperature were modified respectively, followed by an acoustic stage where the pressure term was evaluated implicitly, and the pressure was modified. Pressure Poisson equations was solved by Bi-CGSTAB, and SA-AMG method[27] was used for pre-conditioning. For handling the large-scale computing problem, the methods were parallelized by the domain-decomposition method with MPI.

Regarding the interface tracking method, the following equations could be derived by considering the volume divergence from the interface due to the phase change.

$$\begin{aligned}
&\frac{\partial H_s}{\partial t} + (\vec{u}_s\cdot\nabla)H_S - \frac{\dot{m}}{\rho_{gas}}\vec{n}_s\cdot\nabla H_s = 0, \\
&\frac{\partial H_s}{\partial t} + (\vec{u}_s\cdot\nabla)H_S - \frac{\dot{m}}{\rho_{liq}}\vec{n}_s\cdot\nabla H_s = 0.
\end{aligned} \tag{6}$$

where ρ - density, kg/m^3; $\vec{u}_s$ – interface velocity, m/s; H_s - Heaviside function, -; $\dot{m}$ - phase change rate per unit area, kg/m^2/s; $\vec{n}_s$ - normal vector at the interface, -.

The terms, $\dot{m}/\rho_{gas}\,\vec{n}_s \cdot \nabla H_s$ and $\dot{m}/\rho_{liq}\,\vec{n}_s \cdot \nabla H_s$, represented the change in the discriminant function due to phase change. If there was no phase change, $\dot{m} = 0$ and the velocity of each phase coincided with the velocity at the interface, thus the advection equation (Eq. 6) was a general discriminant function. The interface tracking part employed MARS[28] method which was a kind of PLIC-VOF method. The MARS method was superior to finite volumetric advection of binary functions.

2.2 Phase change model

We proposed 3-stage phase change model[19], as shown in Fig.3. Adopting this 3-stage model enabled treating the phase change phenomenon on a large grid, because each model could treat the different phase change scale. The phase change phenomenon calculation was divided into those that could be captured by CFD and those that were too small to be captured by CFD, the former being calculated directly by CFD and the latter by a sub-grid scale phase change model. The sub-grid scale phase change model consisted of a two-stage model: a wall boiling model was used to simulate the bubble formation at the wall and a temperature recovery-based model[29] was used to simulate the phase change in the liquid phase cell. This two-stage model could calculate the boiling nucleation and growth of small size bubbles which could not be captured by CFD. In CFD calculation, the amount of phase change was obtained by the energy jump condition.

2.2.1 Wall boiling model (1st stage)

In this stage, boiling from a wall at wall cells was calculated. Once the superheat of liquid at wall cells exceeded the bubble growth activation superheat ΔT_{ac}, the bubble nucleation occurred.

$$\Delta T_{ac} = \frac{2\sigma\left(\frac{1}{\rho_{GAS}} - \frac{1}{\rho_{LIQ}}\right)T_{sat}}{L_{vap}}\frac{1}{r_c}, \tag{7}$$

where ΔT_{ac} – bubble growth activation super heat, K; ρ - density, kg/m^3; T_{sat}– saturation temperature, K; σ – surface tension coefficient, N/m; L_{vap} – latent heat, J/kg; r_c – cavity radius, m.

Then, the bubble grew due to heat input from the wall, and the bubble growth rate was calculated by the following Eq. (8).

$$\dot{V} = \frac{1}{\rho_{GAS}}\oint_{Bubble}\dot{m}(\varphi)dS(\varphi) = \frac{2\pi\kappa_{LIQ}(T_{wall}-T_{sat})r_c}{\rho_{GAS}L_{vap}}\log\frac{\varepsilon+\cos\theta}{\varepsilon}. \tag{8}$$

where κ – thermal conductivity, W/m·K; ρ - density, kg/m^3; T_{sat}– saturation temperature, K; T_{wall}– wall temperature, K; ϵ – microlayer thickness, m; L_{vap} – latent heat, J/kg; θ – contact angle, rad; r_c – cavity radius, m.

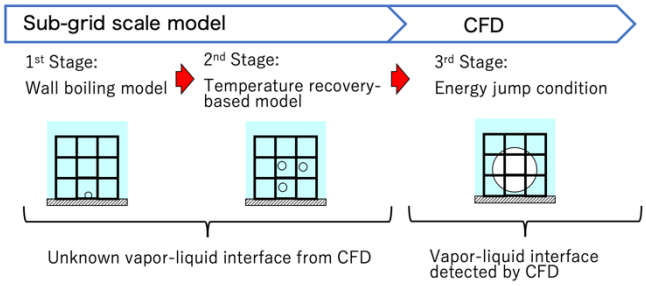

Fig. 3 Phase change model.

In this paper, the cavity radius r_c was set to 3.89μm so that boiling started at 0.01 K of superheat. And the boiling bubble was assumed not to affect each other and to grow independently.

2.2.2 Temperature recovery-based model (2nd stage)

When the bubbles inside the grid cell grew and the gas occupied the 0.1 % volume of the grid cell, the boiling model was transferred to the second stage model based on the temperature recovery method. This model could connect the wall boiling model and direct phase change calculation on CFD. In the previous research, it was found that the wall boiling model was insufficient to provide the amount of boiling on a large grid, leading not to be transferred to CFD calculation. In this method, the amount of boiling in the liquid cell was calculated by Eq. (9).

$$S = \frac{\rho_{liq}\alpha_{liq}C_{pliq}\min\left((T_{LIQ}-T_{sat}),\Delta T_{limit}\right)}{L_{vap}\times dt}, \quad (9)$$

where κ – thermal conductivity, W/m·K; ρ_{liq} – liquid density, kg/m^3; α_{liq}– liquid volume fraction, -; T_{LIQ}– liquid temperature, K; ΔT_{limit} – superheat limit, K; L_{vap} – latent heat, J/kg; dt – time step, sec.

2.2.3 Energy jump condition (3rd stage)

When bubbles were formed and grew and the percentage of gas volume inside the grid cell exceeded 50%, the phase change calculation was moved on to the calculation by CFD.

Based on the energy jump condition at the vapor-liquid interface, the rate of the phase change per unit area $\dot{m}$ in CFD was calculated from Eq. (10). This equation meant that the difference between the heat flux from gas and the one from liquid was used for phase change. The heat flux $\vec{q}$ was calculated from the temperature gradient between the temperature on the grid cell and saturation temperature as shown in Eq. (11). The distance function ϕ from the interface followed the concept of the level set method.

$$\dot{m} = \frac{(\vec{q}_i-\vec{q}_{i+1})\cdot\vec{n}}{L_{vap}}, \quad (10)$$

$$\vec{q} = -\kappa\nabla T \sim -\frac{\kappa(T-T_{sat})}{\phi}\nabla\phi, \quad (11)$$

3. NUMERICAL RESULTS

3.1 30m^3 liquefied hydrogen tank

3.1.1 Numerical condition of 30m^3 liquefied hydrogen tank

In this simulation, the 3-D simulation case was re-evaluated in terms of temperature for understanding the mechanism of the pressure recovery phenomenon. The calculation target was a 3-D computational grid that mimicked the cross-sectional shape of the 30m^3 liquefied hydrogen tank at the JAXA Noshiro Rocket Testing Center with a diameter of 2.3 m and a height of 7.622 m. 3-D stencil in Fig. 4 employed 129 domains with a total of 1,968,131 cells. In this simulation, the minimum edge length of the mesh was approximately 10mm, and thus the influence of turbulence could be ignored. The initial condition was that the liquid level was 6.248 m, the temperature inside the tank was linearly complemented from the experimental data, and the pressure was 321.8 kPaG with hydrostatic pressure on the liquid. The tank wall was set to the isothermal no-slip condition. The isothermal no-slip wall conditions were set to the tank walls, and radial walls for axial symmetry were given slip walls. The outflow velocity boundary condition of both cases was calculated from the experimentally obtained mass flow rate to the upper wall of the tube attached to the tank[19].

3.1.2 Results of 30m³ liquefied hydrogen tank

The time variation of temperature distribution inside the tank was shown in Fig. 5. This figure illustrated that the vapor-liquid interface was the coolest area at the pressure overshoot point, which meant that pressure decrease was dominant due to the boiling delay. After that, the area became the saturation temperature because the boiling bubble stirred the interface. Therefore, this saturated temperature layer formed on the surface of the liquid phase, leading to the equilibrium state.

Figure 6 showed the time variations of temperature at the thermometer position. The temperature of the experiments was obtained from Silicon Diode Sensor (DT-670-CU-1.4L). These results illustrated that the temperature obtained by the experiments was different from the one by CFD. Although the experimental results included measurement errors, the temperature trend in the experiment followed the saturation temperature, on the other hand, in the CFD case, the temperature remained constant. Therefore, it was considered that the boiling from the wall of the thermometer probe made this difference. In experiments and the tanker operations, it was difficult to measure the temperature inside the liquid, and the superheat of the liquid phase was not clear during depressurization.

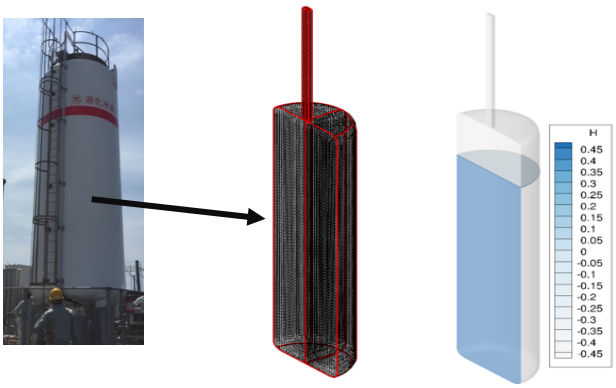

Fig. 4 Schematic of computational domains and initial condition of 30m³ liquefied hydrogen tank (H meant the liquid volume fraction of a cell / -0.5: gas, 0.5: liquid)

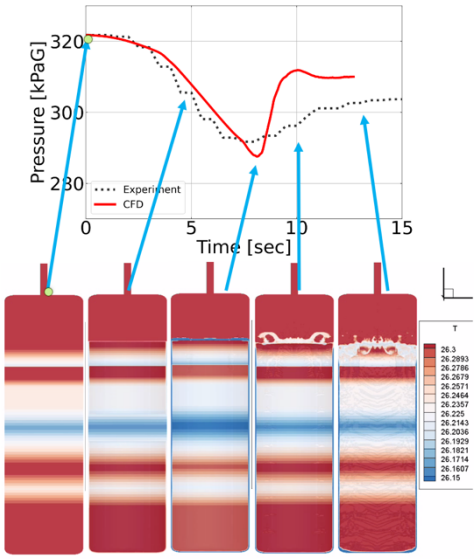

Fig. 5 Time variation of pressure and temperature at the sectional area.

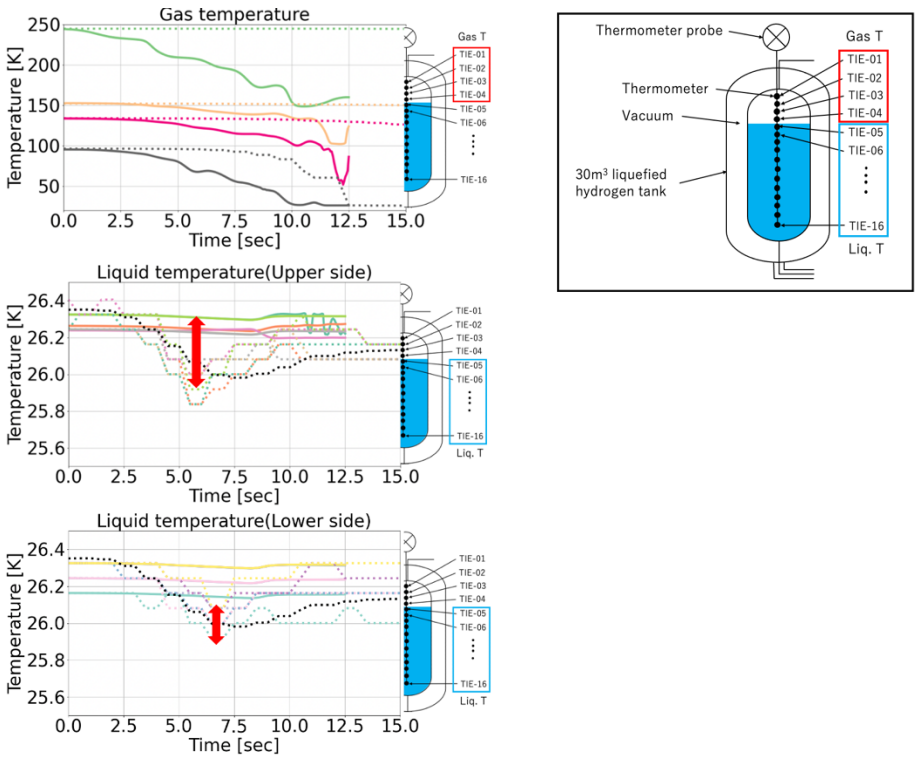

Fig. 6 Time variation of temperature around the beginning of the experiment with schematic of the inside of the 30m^3 tank (Line: CFD results, and dotted line: dotted results). TIE-01~16 meant thermometers. From top to bottom: TIE-01…TIE-16. CFD results were obtained from 3-D calculation. Red arrows showed the gap between the experiment and CFD.

3.2 1250m^3 liquefied hydrogen tank

3.2.1 Numerical condition of 1250m^3 liquefied hydrogen tank

As a preliminary CFD analysis, 2-D CFD of 1250m^3 tank calculation was conducted for investigating the depressurization operation of SUISO FRONTIER. As shown in Fig. 7, This calculation employed a 2-D computational grid that mimicked the cross-sectional shape of the 1250m^3 tank, and the total number of cells were 1,909,720 points. In this simulation, the minimum edge length of the mesh was also approximately 10mm. As a test case, the initial pressure was 321.8 kPaG and the initial temperature of the whole grids was 26.315 K which was around the saturation temperature of the initial pressure.

3.2.2 Preliminary analysis on 1250m^3 liquefied hydrogen tank

The time variation of pressure and visualized results were shown in Fig. 8. The pressure trend was the same as the 30m^3 liquefied hydrogen tank case. At the beginning of depressurization, the pressure decrease was dominant because of the boiling delay, then the pressure recovery occurred caused by a large amount of the boiling bubble. After that, the state inside the tank led to the equilibrium and the pressure became constant. However, the liquid behaviour was more intense than the 3-D CFD results of 30m3 tank, because the 2-D stencil tended to illustrate the boiling phenomenon more intensely[19]. Therefore, as future research, it will be required to conduct a 3-D CFD calculation to validate the effect of tank size and shape.

4. CONCLUSION

The purpose of this paper was to re-evaluate the mechanism of the pressure recovery phenomenon in terms of temperature and clarify the depressurization operation of SUISO FRONTIER.

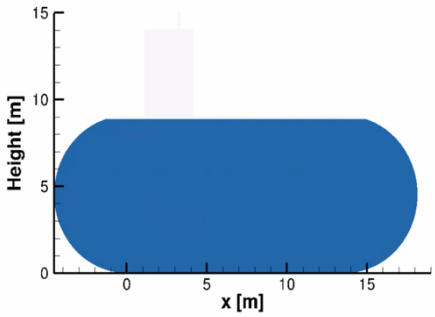

Fig. 7 Schematic of 2-D computational domains and initial condition of the 1250m^3 tank.

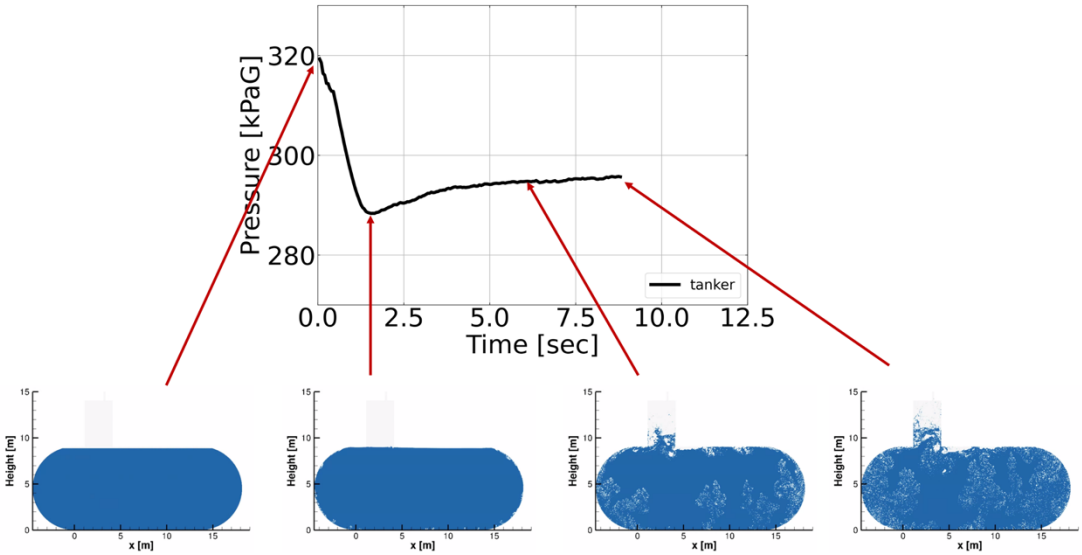

Fig. 8 Time variation of pressure and visualized results of liquid behaviour

For understanding the mechanism of pressure recovery phenomenon, the 3-D CFD analysis was re-evaluated in terms of temperature and boiling model. The results illustrated that the boiling delay caused the pressure recovery phenomenon, and the evolved bubbles stirred the vapor-liquid surface and led to the equilibrium state inside the tank. For clarifying the phenomenon inside the 1250m^3 liquefied hydrogen tank of SUISO FRONTIER, 2-D CFD calculation was conducted as a preliminary study. The results showed that the pressure trend was the same as the 30m3 tank and the pressure recovery occurred in a certain condition. However, 2-D stencil illustrated that the liquid behavior was more intense and liquid level increased; thus 3-D CFD calculation was needed to understand the liquid behavior.

REFERENCE

[1] J. Andersson and S. Grönkvist, “Large-scale storage of hydrogen,” *Int. J. Hydrogen Energy*, vol. 44, no. 23, pp. 11901–11919, 2019, doi: 10.1016/j.ijhydene.2019.03.063.

[2] Hydrogen and Fuel Cells Strategy Office, Advanced Energy Systems and Structure Division, Energy Conservation and Renewable Energy Department, Agency for Natural Resources and Energy Japan, “Basic Hydrogen Strategy,” pp. 1–37, 2017, [Online]. Available: http://www.meti.go.jp/english/press/2017/pdf/1226_003b.pdf.

[3] S. Kamiya, M. Nishimura, and E. Harada, “Study on introduction of CO2 free energy to Japan with liquid hydrogen,” in *25th International Cryogenic Engineering Conference and the International Cryogenic Materials Conference in 2014, ICEC 25–ICMC 2014*, 2015, vol. 67, pp. 11–19, doi: 10.1016/j.phpro.2015.06.004.

[4] S. Unno, T. Umemura, H. Kagaya, and Y. Takaoka, “Clarification of hazardous areas applied to newly developed liquefied hydrogen carrier,” in *Proceedings of the International Offshore and Polar Engineering Conference*, 2018, pp. 876–880.

[5] Y. Takaoka, A. Saeed, K. Nishifuji, and K. Kanbe, “Design and Operation of the First LH2 Carrier,” in *Gastech 2019 Exhibition & Conference*, 2019, pp. 1–10.

[6] Kawasaki Heavy Industries, Ltd., *KAWASAKI TECHNICAL REVIEW*, vol. 182. Hiroshi, Nakatani, 2021.

[7] O. Miyatake, K. Murakami, Y. Kawata, and T. Fujii, “Fundamental Experiments of Flash Evaporation,” *Bull. Soc. Sea Water Sci. Japan*, vol. 26, no. 4, pp. 189–198, 1972, doi: 10.11457/swsj1965.26.189.

[8] O. Miyatake, T. Fujii, T. Tanaka, and T. Nakaoka, “Flash evaporation phenomena of pool water,” *Kagaku Kogaku Ronbunshu*, vol. 1, no. 4, pp. 393–398, 1975, doi: 10.1252/kakoronbunshu.1.393.

[9] D. Saury, S. Harmand, and M. Siroux, “Experimental study of flash evaporation of a water film,” *Int. J. Heat Mass Transf.*, vol. 45, pp. 3447–3457, 2002, [Online]. Available: www.elsevier.com/locate/ijhmt.

[10] D. Saury, S. Harmand, and M. Siroux, “Flash evaporation from a water pool: Influence of the liquid height and of the depressurization rate,” *Int. J. Therm. Sci.*, vol. 44, pp. 953–965, 2005, doi: 10.1016/j.ijthermalsci.2005.03.005.

[11] D. Zhang, D. Chong, J. Yan, and Y. Zhang, “Study on steam-carrying effect in static flash evaporation,” *Int. J. Heat Mass Transf.*, vol. 55, pp. 4487–4497, Aug. 2012, doi: 10.1016/j.ijheatmasstransfer.2012.03.013.

[12] C. Wang, R. Xu, X. Chen, P. Jiang, and B. Liu, “Study on water flash evaporation under reduced pressure,” *Int. J. Heat Mass Transf.*, vol. 131, pp. 31–40, Mar. 2019, doi: 10.1016/j.ijheatmasstransfer.2018.11.009.

[13] H. C. Hewitt and J. D. Parker, “Bubble Growth and Collapse in Liquid Nitrogen,” *J. Heat Transfer*, vol. 90, no. 1, pp. 22–26, Feb. 1968, doi: 10.1115/1.3597454.

[14] Y. Shingo, H. Yutaka, and T. Ikuo, “An Experimental Study on Flashing Phenomenon of Liquid Nitorgen,” *Trans. Japan Soc. Mech. Eng. Ser. B*, vol. 58, no. 549, pp. 1498–1503, 1992.

[15] W. Toshiaki, H. Yutaka, and T. Ikuo, “Flashing Phenomena of Liquid Nitrogen in a Pressure Vessel,” *Trans. Japan Soc. Mech. Eng. Ser. B*, vol. 61, no. 585, pp. 1849–1854, 1995.

[16] W. Toshiaki, H. Yutaka, and T. Ikuo, “Flashing Phenomena of DepressuTized Liquid Nitrogen in a Pressure Vessel,” *Trans. Japan Soc. Mech. Eng. Ser. B*, vol. 63, no. 610, pp. 2148–2153, 1997.

[17] M. Takeda, T. Usui, and K. Maekawa, “Study on boiling behavior of pressurized liquid nitrogen under rapid depressurization,” *IOP Conf. Ser. Mater. Sci. Eng.*, vol. 502, no. 1, 2019, doi: 10.1088/1757-899X/502/1/012092.

[18] K. Tani *et al.*, “Prediction of Pressure Reduction Rate in 30m3 Liquid Hydrogen Tank Based on Experimental And Numerical Analysis,” in *International Conference on Hydrogen Safety 2019*, 2019, pp. 1–12.

[19] K. Tani *et al.*, “Pressure recovery during pressure reduction experiment with large-scale liquid hydrogen tank,” *Int. J. Hydrogen Energy*, 2021, doi: 10.1016/j.ijhydene.2020.12.184.

[20] T. Himeno, T. Watanabe, and A. Konno, “Numerical analysis of two-phase flow behavior in a liquid propellant tank,” Jun. 1999, doi: 10.2514/6.1999-2177.

[21] T. HIMENO, H. NEGISHI, S. NONAKA, C. INOUE, T. WATANABE, and S. UZAWA, “Numerical Analysis of Free-Surface Flows under Various Conditions in Acceleration : Improvement of CIP-LSM : CIP-Based Level Set & MARS(The Forefront of Multi-Physics CFD/EFD),” *Trans. Japan Soc. Mech. Eng. Ser. B*, vol. 76, no. 765, pp. 778–788, 2010, doi: https://doi.org/10.1299/kikaib.76.765_778.

[22] Y. Umemura *et al.*, “Liquid nitrogen chill-down process prediction by direct interface tracking approach,” *53rd AIAA/SAE/ASEE Jt. Propuls. Conf. 2017*, no. July, pp. 1–12, 2017, doi: 10.2514/6.2017-4761.

[23] Y. Umemura, T. Himeno, and T. Watanabe, “Numerical analysis of boiling flow in surface-tension-dominated environment,” *49th AIAA/ASME/SAE/ASEE Jt. Propuls. Conf.*, vol. 1 PartF, pp. 1–14, 2013, doi: 10.2514/6.2013-3843.

[24] M. Sussman and E. G. Puckett, “A Coupled Level Set and Volume-of-Fluid Method for Computing 3D and Axisymmetric Incompressible Two-Phase Flows,” *J. Comput. Phys.*, vol. 162, no. 2, pp. 301–337, 2000, doi: 10.1006/jcph.2000.6537.

[25] S. Osher and J. A. Sethian, “Fronts propagating with curvature-dependent speed: Algorithms based on Hamilton-Jacobi formulations,” *J. Comput. Phys.*, vol. 79, no. 1, pp. 12–49, 1988, doi: 10.1016/0021-9991(88)90002-2.

[26] T. Yabe and E. Takei, “A New Higher-Order Godunov Method for General Hyperbolic Equations,” *J. Phys. Soc. Japan*, vol. 57, no. 8, pp. 2598–2601, Aug. 1988, doi: 10.1143/JPSJ.57.2598.

[27] P. Vaněk, J. Mandel, and M. Brezina, “Algebraic multigrid by smoothed aggregation for second and fourth order elliptic problems,” *Computing*, vol. 56, no. 3, pp. 179–196, 1996, doi: 10.1007/BF02238511.

[28] T. Kunugi, “MARS for Multiphase Calculation,” *Comput. Fluid Dyn. J.*, vol. 9, pp. 563–571, 2001, Accessed: May 13, 2020. [Online]. Available: http://ci.nii.ac.jp/naid/10025476591/ja/.

[29] T. Kunugi, N. Saito, Y. Fujita, and A. Serizawa, “Direct numerical simulation of pool and forced convective flow boiling phenomena,” in *Proceedings of the Twelfth International Heat Transfer Conference*, 2002, no. 3, pp. 497–502, doi: 10.1615/ihtc12.2290.